Forest Chemicals Review
www.forestchemicalsreview.com
ISSN: 1520-0191
September-October 2022 Page No. 289-305
Article History: Received: 05 April 2022, Revised: 27 April 2022, Accepted: 03 May 2022, Publication: 14 May 2022

Output Performance of Flexible Ecoflex Film Based Triboelectric Nanogeneration during Friction Process

Zhaoqi Qu[1*], Guanggui Cheng[1], Jie Cao[1], Shengping Dai[1], Lei Han[1], Yan Zhong[1], Zhongqiang Zhang[1]

[1] Institute of Intelligent Flexible Mechatronics, Jiangsu University, Zhenjiang, Jiangsu 212013, China
*Corresponding Author.

Abstract:

The output performances of triboelectric nanogenerator (TENG) are influenced by several parameters such as contact area, material properties, and surface topography etal. However, the influence of friction process on its output performance is not clear. In this work, a TENG worked in slide mode was prepared by flexible Ecoflex00-30 film and aluminum foil electrode. A test apparatus was designed to study the tribological properties and the corresponding output performance of the Ecoflex00-30 film-aluminum foil friction pair with different load and speed. It was found that the working process can be divided into four stages, namely, running-in, initial wear, stable wear, and severe wear stages. In the running-in stage, the electrical output performance of TENG significantly improved with the extension of the test time due to the accumulation of polymer surface charges and the elastic deformation caused by the electrostatic interaction force. In the initial wear stage, an abrasion microstructure was produced on the polymer surface, resulting in an increase in the contact area and slow growth of the electrical output performance. In the stable wear stage, the contact area further increased during the wearing process, and in the meantime, amount of transfer film formed on the electrode surface, which resulting in a stable electrical output when a dynamic balance is achieved. In the severe wear stage, fatigue wears results in pitting formation on the film surface due to the continuous stress cycle, and the electrical output is significantly reduced with the rapidly reduction of contact area.

Keywords*: Triboelectric nanogenerator, Flexible film, Electrical output, Friction process*

I. INTRODUCTION

Triboelectric nanogenerators (TENGs) can efficiently convert mechanical energy into electrical energy via the triboelectric effect and electrostatic induction principle, and which have received great attention as new energy harvesting technologies. The current research on TENGs mainly focuses on the structural design [1-3] and performance improvement [4-6]. Many scholars have proposed innovative structures for the collection of ocean energy [7], wind energy [8], vibrational energy [9-11], and human motion energy [12-15]. Research on the output performance improvement mainly focuses on the following: Improved

Forest Chemicals Review
www.forestchemicalsreview.com
ISSN: 1520-0191
September-October 2022 Page No. 289-305
Article History: Received: 05 April 2022, Revised: 27 April 2022, Accepted: 03 May 2022, Publication: 14 May 2022

output performance [16-20], wear resistance [21, 22], longevity [23]. Xu et al. [24] used a floating layer structure and a charge pump to increase the surface charge density of the friction layer for improving the output performance of TENG. Li et al. [25] showed a high-output TENG with a rotating contact-separation structure that combines rectification and phase difference. Zhang et al. [26] performed surface chemical modification with an oleic acid-enhanced triboelectric nanogenerator with high wear resistance. Wu et al. [27] showed that the use of liquid lubrication can effectively improve the wear resistance of TENG and prolong its service life. However, seldom study has been conducted on the life and wear failure mechanism of TENG to date even though the wear and surface degradation of TENG are occasionally mentioned in the literature.

In order to explore the relationship between the tribological properties of the flexible polymer and the electrical output performance during the friction process, here in this paper, a friction test platform was designed and fabricated, and the typical Ecoflex00-30 polymer and aluminum foil electrode were selected as the research objects. The test analyzes the change trend of the tribological performance and electrical output of TENG during the friction process. Furthermore, this test is carried out to study the influence of load, speed, and durian time on the open circuit voltage, short circuit current, transferred charge and cumulative wear, which provides reference for the design of long-life and high-reliability TENG.

II. EXPERIMENTAL SECTION

2.1 Test Experiment Platform

In accordance with the test requirements, we built the test platform shown in Figure 1a to examine the tribological and electrical output properties of TENG. The test platform includes a movable stage, roulette, a slide screw, a stepping motor, a holding fixture, a controller, and a PC, oscilloscope composition and an electrometer. During the experiment, several parameters such as load and speed, is completed with the self-built controller and PC. The output end is connected to the oscilloscope to realize real-time data monitoring and recording. Figure 1b shows the schematic of the movable test platform and the turntable. The test sample is fixed on the test platform by a fixture. The conductive slip ring is used to prevent the wire from being entangled with the rotation of the wheel.

The specific workflow of the test platform is as follows: First, the known parameters in the movable stage are weighed for sensor calibration. The sample was then clamped on a movable loading platform, and the parameters of motor 1 and motor 2 were set by PC. The experimental test is carried out after the required load and speed are set. The force sensor obtains the pressure and friction signals, which are collected and sent to the PC by the single-chip microcomputer, while the corresponding output voltage is recorded in real time by an oscilloscope.

Forest Chemicals Review
www.forestchemicalsreview.com
ISSN: 1520-0191
September-October 2022 Page No. 289-305
Article History: Received: 05 April 2022, Revised: 27 April 2022, Accepted: 03 May 2022, Publication: 14 May 2022

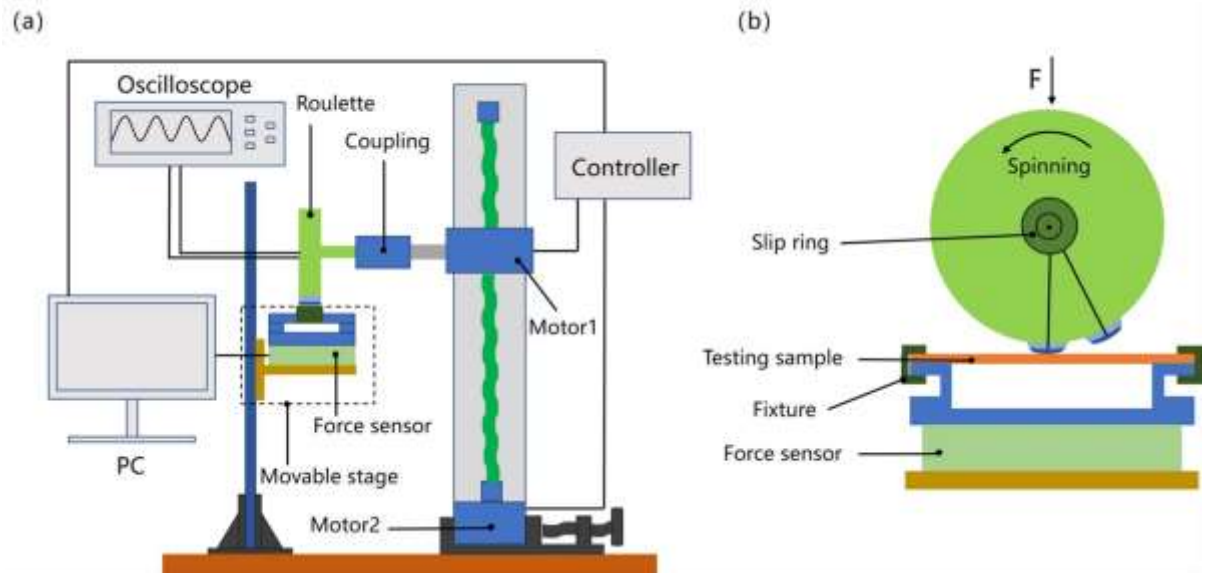

Fig 1: Detail information of the test platform. (a) Schematic diagram of friction test platform; (b) Schematic diagram of movable stage and roulette in test state

2.2 Sample Preparation

Ecoflex00-30 polymer material was selected in this experiment as the research object. The commercial AB glue was mixed at a ratio of 1:1 and vacuumed for 10 min. Then, the mixture was placed on a homogenizing table and homogenized for approximately 30 s at a rotation speed of 200 r/min. After curing for 3 h at 25 °C, a Ecoflex00-30 film with a thickness of 500 μm was prepared, and the film was cut into several 15×80 mm test samples for further use.

2.3 Experimental Process

The test was performed at room temperature (25±1 °C) in an ambient condition (with 40%–50% relative humidity). First, the test sample was ultrasonically cleaned for 10 min and then dried in a blast drying oven for 5 min. Subsequently, the test sample was weighed and recorded. Thereafter, the test sample was placed in a friction test platform. The different loads (0, 10, and 20 mN) and speed (30, 60, and 90 r/min) conditions of friction were applied on the test platform. During the test, the electrical output was recorded in real time, and the samples were taken out for weighing followed by washing, drying after 10, 40, 70, 100, 130 and 160 min from the start of the experiment. The surface morphology was observed by employing a fluorescence microscope, and a Raman spectrometer was used to characterize the material transfer on the electrode surface. After the recording and characterization, the sample was fixed in place to continue the experiment. Each experiment was repeated three times, and the electrical output, load, speed and other information were recoded for analyzing.

Forest Chemicals Review
www.forestchemicalsreview.com
ISSN: 1520-0191
September-October 2022 Page No. 289-305
Article History: Received: 05 April 2022, Revised: 27 April 2022, Accepted: 03 May 2022, Publication: 14 May 2022

III. RESULTS AND DISCUSSION

3.1 Influence of Friction Time on the Electrical Output and Tribological Characteristics of the TENG

Figure 2a shows electrical output and weight loss verse time of the entire working process of the TENG with applied load of 10 mN, and rotation velocity of 60r/min. it is found that the whole process can be divided into four stages, namely, running-in, initial wear, stable wear and severe wear stages.

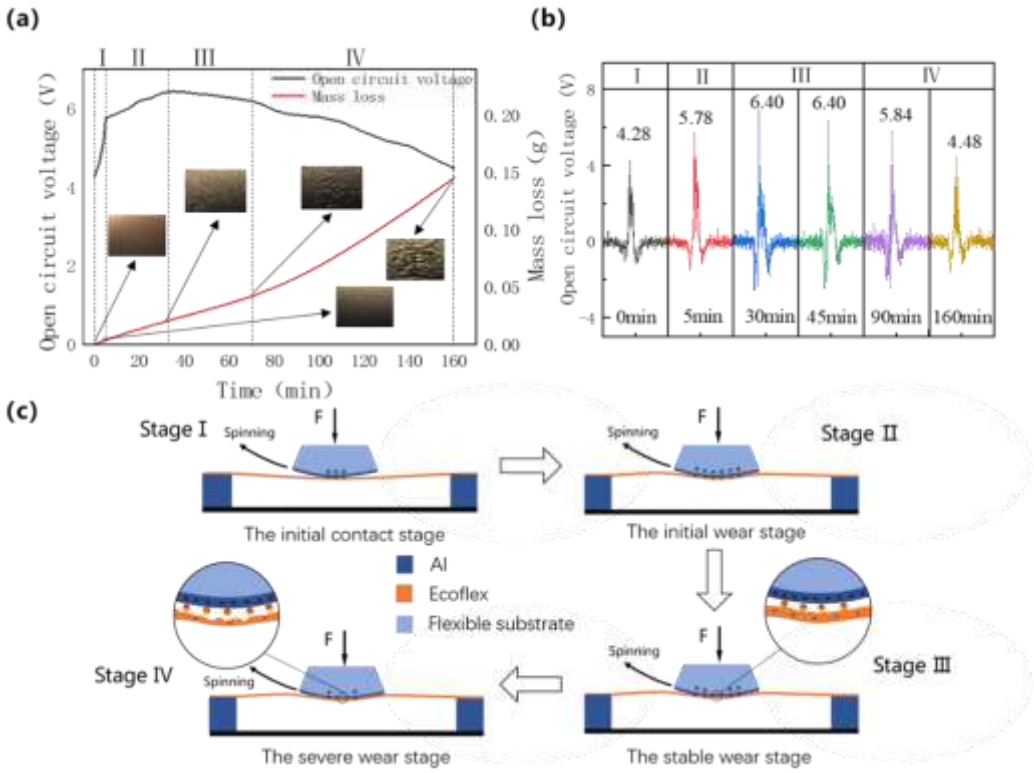

Fig 2: The test process and results under the test conditions of 10mN and 60r/min (a) The output voltage and cumulative mass loss of the friction test change with time and inset graphs show the typical morphology of the surface of the test sample at each stage; (b) Real-time output waveform diagram at different time points; (c) Schematic diagram of the friction test process. At stage I, the aluminum foil is contact with the test sample. At the stage II, the charge transfers increase with the increase of the contact area. Stage III, the silica peels off and adheres to the surface of the aluminum foil to form a transfer film that affects the charge transfer. At stage IV, the continuous stress cycle causes defects on the surface of the silica gel. The contact area decreases and the amount of charge transferred decreases accordingly.

3.1.1 Running-in stage

The running-in phase occurred within 3–5 min from the beginning of the test, and the output voltage increased by approximately 30% from the initial 4.48 V to 5.86 V. First, the output voltage increased due

Forest Chemicals Review
www.forestchemicalsreview.com
ISSN: 1520-0191
September-October 2022 Page No. 289-305
Article History: Received: 05 April 2022, Revised: 27 April 2022, Accepted: 03 May 2022, Publication: 14 May 2022

to the accumulation of electric charge with the repeated friction between the polymer material and the electrode. The two contact surfaces attracted each other due to the electrostatic force, resulting in the increase in the actual contact area, and which promoted further accumulation of electric charge [28], result in the enhanced electrostatic induction, the attraction effect of the electrostatic force gradually increased. The attraction phenomenon between the Ecoflex film and the electrode can be clearly observed.

The experiments verified that the main reason for the increase in output voltage during the running-in phase is the combined action of load force and electrostatic force, which has little to do with the changes in surface topography. Specific verification method: The electrical output significantly increased within 2 min from the start of the experiment. The test sample was removed, and the surface morphology was observed. The surface morphology showed only microscopic scratches, and no other obvious morphological changes were evident, as shown in the inset in Figure 2a. The wear rate of running and phase times was estimated to be approximately 1 mg/min from the cumulative volume curve.

3.1.2 Initial wear stage

The initial stage occurred in the time period of 5–30 min, the output voltage increased from 5.86 V to 6.44 V, and the growth rate was approximately 9%, showing a slow growth trend. At this stage, the charge accumulation reached saturation, the electrostatic force was stable and did not change much, and the increase in output was mainly due to the increase in area caused by the sliding friction of the surface. The initial wear smoothened the peaks between the film and the electrode, and microstructures appeared on the film surface, increasing the actual contact area between the film and the electrode surface. At this stage, the surface of the silica gel gradually appeared scaly when seen via a microscope. The amount of cutting wear was relatively stable, and the wear rate was approximately 0.73 mg/min, which was slightly lower than that in the running-in stage.

3.1.3 Stable wear stage

The stable wear stage occurred in the time period of 30–70 min, and the output was stable at approximately 6.4 V; however, a slight drop of 4% was evident. The main reason for the decrease in output stability is that the surface of the silica gel peeled off due to continuous friction at this stage, resulting in a layer of transfer film attached to the surface of the aluminum foil electrode [29]. On the one hand, the appearance of the transfer film makes the lubrication state between the film and the electrode good, and the wear volume is reduced. The morphology change was reduced, and the wear rate at this stage dropped to approximately 0.64 mg/min. On the other hand, the amount of charge transfer decreased due to the blocking effect of the transfer film, which is opposed to the continuous sliding friction leading to the increase in the contact area. The final performance is that the output voltage drops by about 3%. The transfer film gradually stabilized with the wear progress. We selected a certain amount of metal electrodes to further confirm the occurrence of the transfer film and analyzed the surface morphology of the metal electrodes with a scanning electron microscope and a Raman spectrometer. The SEM image and Raman test shown in Figure 3 can also confirm the role of the transfer film in the friction and wear process. At this

Forest Chemicals Review
www.forestchemicalsreview.com
ISSN: 1520-0191
September-October 2022 Page No. 289-305
Article History: Received: 05 April 2022, Revised: 27 April 2022, Accepted: 03 May 2022, Publication: 14 May 2022

stage, the electrostatic force tended to be stable, and the morphology was mainly scaly, accompanied by slight pitting and peeling.

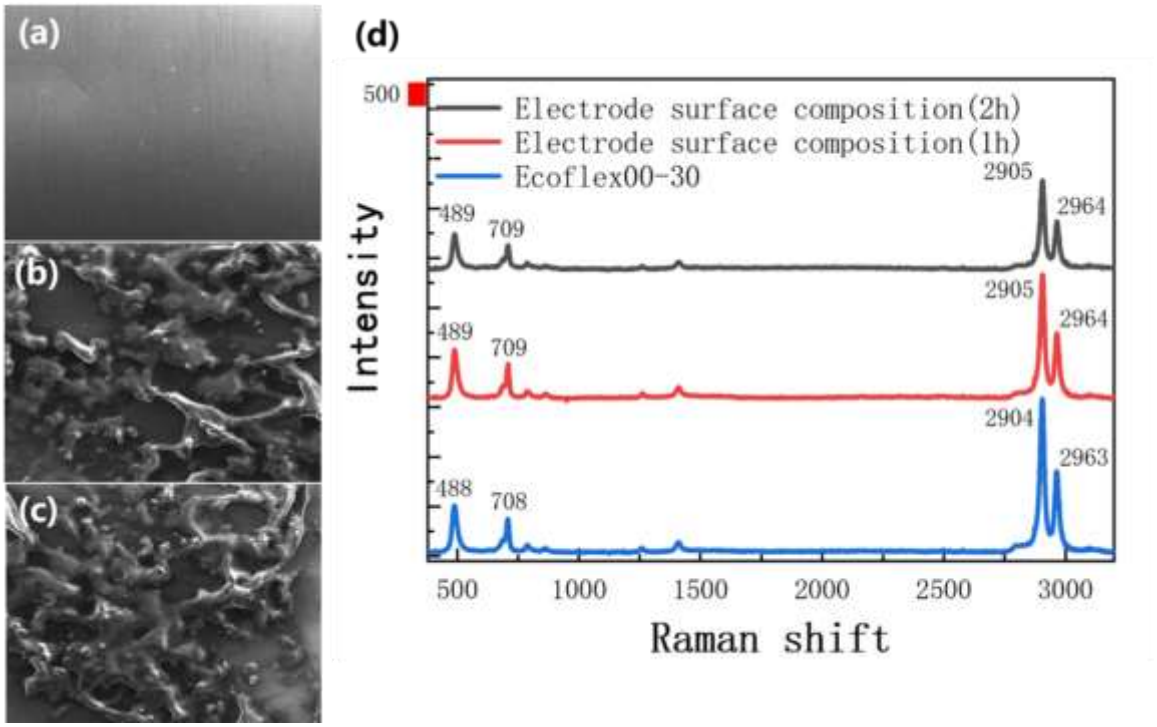

Fig 3: The proof of the existence of transfer film (a) SEM image of pure aluminum film surface; (b) SEM image of aluminum surface in friction test for 1h; (c) SEM image of aluminum foil surface in friction test for 2h; (d) Comparison of surface composition of aluminum foil and pure Ecoflex00-30 Raman for 1h and 2h of friction test.

3.1.4 Severe wear stage

The severe wear stage occurred 70 min after the start of the test, and the output voltage of this stage showed a downward trend. The downward trend became more obvious with the increase in the test time. The main reasons for the drop in output voltage are fatigue and wear caused by long-term stress cycles. The drastic area change breaks the balance of the stable wear stage. At this stage, obvious pitting and peeling phenomenon formed on the surface of silica gel, reducing the actual contact area between the film and the electrode. A similar bonding phenomenon occurred under high-speed and heavy-load conditions, and the amount of wear drastically increased. The average wear rate also significantly increased compared with that in the previous stage, which is approximately 2.18 mg/min.

We stipulate that when the test output voltage drops to 70% of the stable phase, it is deemed to enter the failure phase. This time node is defined as the failure time. In the current test, when the test was carried out for 160 min, the output dropped to 4.5 V, which is 70% of the stable voltage of 6.4 V. Therefore, we believe that 160 min is the failure time under the test conditions of 10 mN and 60 r/min.

Forest Chemicals Review
www.forestchemicalsreview.com
ISSN: 1520-0191
September-October 2022 Page No. 289-305
Article History: Received: 05 April 2022, Revised: 27 April 2022, Accepted: 03 May 2022, Publication: 14 May 2022

3.2 Theoretical Model and Numerical Analysis

In accordance to explain the change process and influencing factors of the friction test, we established the theoretical mechanical and theoretical electrical models of the TENG as shown in Figure 4.

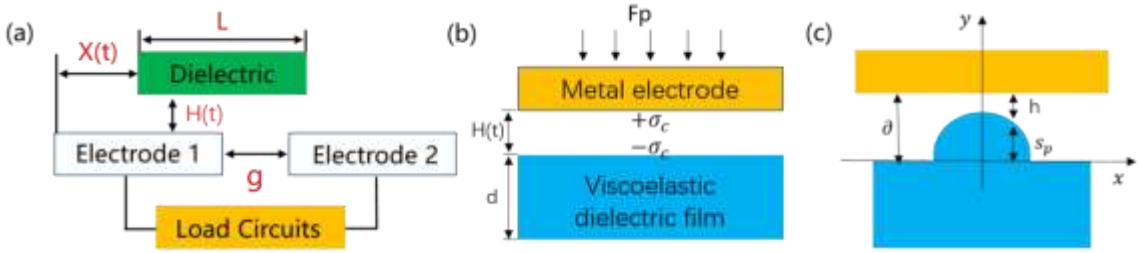

Fig 4: The theoretical model of the friction test structure. (a) Theoretical electrical output model; (b) Theoretical mechanical model; (c) Partially enlarged schematic diagram of the mechanical model

The theoretical model of this tribo-tested electrical output can be simplified as a free-standing layered TENG [30, 31] as shown in Figure 4(a). Since the electric potential on the surface of the dielectric is not constant, the electrical output is analyzed by applying the principle of superposition of potentials using the node concept. Assume that the actual contact area S_C between the dielectric layer and the electrode contains triboelectric charges. According to the principle of superposition of electric fields, the amount of transferred charge can be expressed as:

$$Q_{sc} = \int_0^L \frac{\sigma S_c}{1+(\frac{C_2}{C_1})_{x=g+L}} - \int_0^L \frac{\sigma S_c}{1+(\frac{C_2}{C_1})_{x=0}} \quad (1)$$

where C1, C2 represent the capacitance between the dielectric and electrodes 1, 2.

From formula (1), it can be known that when the dielectric layer slides between the two electrodes and is at the extreme positions at both ends (x=0 and x=g+L), the transferred charge *Qsc* can reach the maximum value, the maximum value *Q*sc,max = σS_C. According to the relationship between the transferred charge *Qsc*, the maximum open circuit voltage *Voc*, and the short circuit current *Isc*:

$$V_{oc} = \frac{Q_{sc}}{C_0} = \frac{\sigma S_c}{C_0} = \frac{4\pi k \sigma S_c g}{\varepsilon s_a} \quad (2)$$

$$I_{sc} = \frac{dQsc}{dt} \quad (3)$$

It can be known that when the structural parameters of the device are fixed, the amount of transferred charge *Qsc*, the open circuit voltage *Voc*, and the short circuit current *Isc* are mainly related to the actual

Forest Chemicals Review
www.forestchemicalsreview.com
ISSN: 1520-0191
September-October 2022 Page No. 289-305
Article History: Received: 05 April 2022, Revised: 27 April 2022, Accepted: 03 May 2022, Publication: 14 May 2022

contact area SC and contact time.

Therefore, a mechanical model is established to discuss the force condition of the model and the influencing factors of the actual contact area. The tested mechanical model can be approximated as a viscoelastic contact model as shown in Figure 4(b). According to the principle of elastic-viscoelastic correspondence, the deformation formula of viscoelastic material can be expressed as:

$$u(x,y,t) = \int_0^t \int_{-\infty}^{+\infty} \int_{-\infty}^{+\infty} K(\Delta x, \Delta y, \Delta t) \frac{\partial F_{ah}(x',y',\xi)}{\partial \xi} dx' dy' d\xi \quad (4)$$

where K() function is the influence coefficient of viscoelastic contact. The Fah() function represents the adhesive contact pressure between the contact surfaces at time t.

Contact adhesion contact pressure mainly includes van der Waals force *Fvdw* and repulsion force *Frep* and electrostatic force *Fele*, which can be expressed as:

$$F_{vdw} = -\frac{H}{6\pi h^3(x,y,t)} \quad (5)$$

$$F_{rep} = \frac{Hl_0^6}{90\pi h^9(x,y,t)} \quad (6)$$

$$F_{ele} = -\frac{\sigma_c^2}{2\varepsilon_0}\left(\frac{B}{B+h(x,y,t)}\right)^2, (x,y) \in \Omega \quad (7)$$

where H represents the intrinsic constant, where ε0 is the dielectric constant of the vacuum, B is the effective thickness constant and Ω is the contact area for the bonding pressure.

Therefore, the adhesive contact pressure can be expressed as:

$$F_{ah} = F_{vdw}(x,y,t) + F_{rep}(x,y,t) + F_{ele}(x,y,t), (x,y) \in \Omega \quad (8)$$

The effective contact area *Sc* of the dielectric film and the metal electrode participates in the contact charging. So the total adhesion interaction force between the metal electrode and the dielectric film can be expressed as:

$$F_{ah}(t) = \iint_{S_c} F_{ah}(x,y,t) dx\, dy \quad (9)$$

It can be known from the above formula (9) that the total adhesive force is a function of the actual contact area and the adhesive contact pressure, so the total contact stress is directly affected by the actual contact area. However, the actual contact area during the friction test is not only affected by the adhesive contact pressure, but also by the continuous friction loss between the dielectric film and the metal electrode. The actual loss of contact area due to wear of the contact surface is difficult to calculate directly, so we use

Forest Chemicals Review
www.forestchemicalsreview.com
ISSN: 1520-0191
September-October 2022 Page No. 289-305
Article History: Received: 05 April 2022, Revised: 27 April 2022, Accepted: 03 May 2022, Publication: 14 May 2022

the volume wear rate to represent the damage to the surface of the dielectric film. There are mainly two types of wear in the friction and wear process: adhesive wear caused by adhesive contact and fatigue wear caused by periodic sliding. According to Akkad's Law [32], the volume wear rate can be expressed as:

$$W_{ad} = \mathrm{k_{ad}} \frac{F}{3\sigma_s} \tag{10}$$

$$W_{sf} = \mathrm{k_{sf}} \frac{F}{3\sigma_s} \tag{11}$$

Where Kad indicates that the dimensionless wear coefficient is related to material properties, and Ksf indicates that the fatigue wear coefficient is mainly related to the number of cycles of material fatigue failure stress. F represents the load force, in this model F=Fp+Fah, σs represents the yield strength of the dielectric film.

Based on the above theoretical analysis, it can be concluded that the main factors affecting the electrical output include the actual contact area and contact time, and the actual contact area is related to the contact force and the number of contact friction cycles. Therefore, from the perspectives of contact load force and contact speed, the influence on the electrical output and friction and wear of the friction test will be discussed respectively.

3.3 Influence of Load on the Output Voltage, Accumulated Wear Amount, Wear Morphology, and Phase Change Trend

It can be seen from Figure 5 that the open-circuit voltage, short-circuit current, transferred charge and accumulated wear amount change with time under the same rotational speed and different load conditions. It can be seen that with the increase of load, the electrical output and wear amount will increase accordingly. The reason for these is that the increase in the load force deforms the flexible dielectric film, resulting in an increase in the actual contact area between the dielectric film and the electrodes. When the actual contact area increases, the total amount of transferred charge increases, which can be seen by observing the charge amount curves in Figures 5(c) and 5(e). The short-circuit current and open-circuit voltage will also increase, and the corresponding curve in Figure 5 can also be seen. At the same time, with the increase of the load, the wear amount also showed the same growth trend. From the surface fluorescence microscope images of 10mN load and 20mN load at the same time node at the same speed in Figure 6, it can be seen that with the increase of load, the surface of the dielectric film appears more obvious wear phenomenon. The greater the load, the greater the accumulated wear and the faster the increase of the accumulated wear.

Forest Chemicals Review
www.forestchemicalsreview.com
ISSN: 1520-0191
September-October 2022 Page No. 289-305
Article History: Received: 05 April 2022, Revised: 27 April 2022, Accepted: 03 May 2022, Publication: 14 May 2022

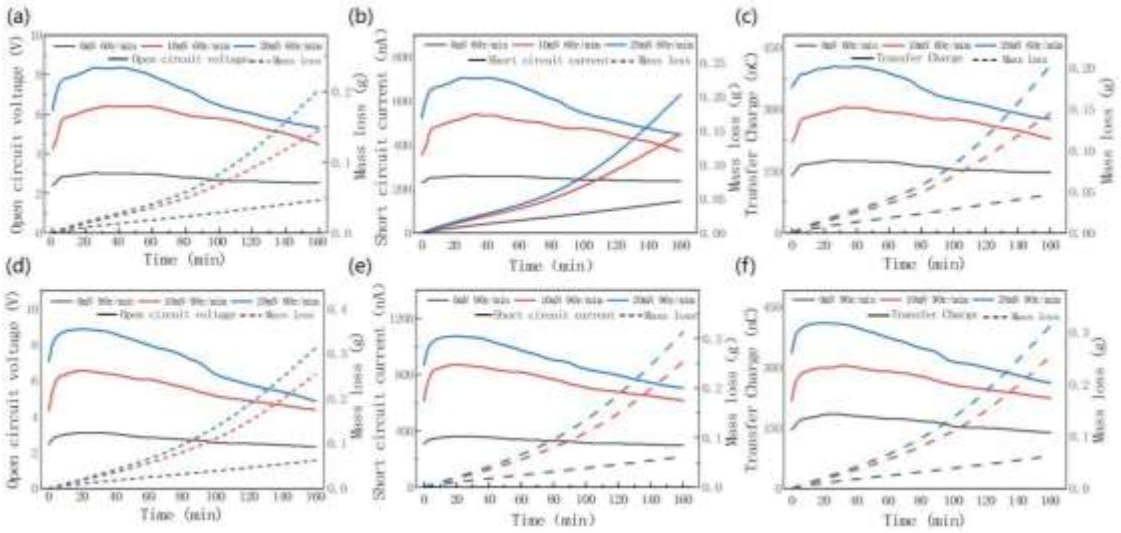

Fig 5: The influence of different loads on the open-circuit voltage, short-circuit current, transferred charge and accumulated wear under the same rotational speed. (a-c) Change curves of open-circuit voltage, short-circuit current, transferred charge and mass loss under different load conditions when the rotational speed is the same as 60r/min; (d-f) Change curves of open-circuit voltage, short-circuit current, transferred charge and mass loss under different load conditions when the rotational speed is the same as 60r/min;

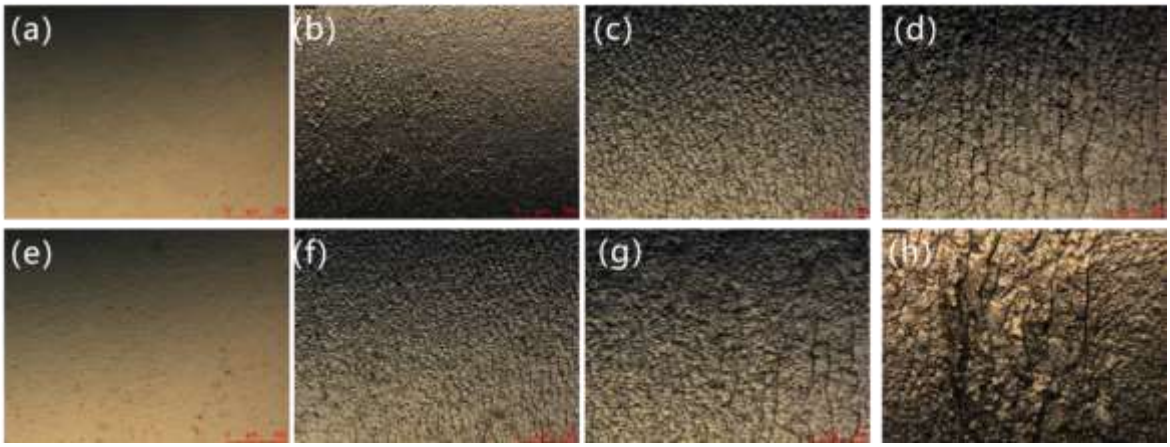

Fig 6: Comparison of surface morphologies of polymer films under the same rotational speed and different loading conditions. (a-d) Fluorescence microscope images of the surface topography of the untested sample, tested 10 min, tested 40 min and tested 70 min under the condition of rotating speed 60 r/min and loading 10 mN; (e-h) Fluorescence microscope images of the surface topography of the untested sample, tested 10 min, tested 40 min and tested 70 min under the condition of rotating speed 60 r/min and loading 20 mN;

The impact of the load on the test is also manifested in the following two points. One is that with the increase of the load, the output improvement of the running-in stage first and then decreases. The improvement of the electrical output in the running-in stage is the focus of our attention. Comparing the

Forest Chemicals Review
www.forestchemicalsreview.com
ISSN: 1520-0191
September-October 2022 Page No. 289-305
Article History: Received: 05 April 2022, Revised: 27 April 2022, Accepted: 03 May 2022, Publication: 14 May 2022

output curves under the same test conditions of 60 r/min, it is found that when the load was increased from 0 mN to 20 mN, the improvement of the transfer charge in the first stage first increased from 17% of 0mN to 26% of 10 mN and then decreased to 16% of 20 mN, the open circuit voltage increased from 15% of 0 mN to 31% of 10 mN and then decreased to 24% of 20mN. This phenomenon is due to the change in the output of the first stage I mainly because of the coupling of the loading force and the electrostatic force. The elastic deformation of the polymer film under the action of the coupling force and the electrostatic adhesion effect caused the actual contact area of the film and the electrode to change, which ultimately affects the output voltage. Under the test condition of 0 mN, the load force does not participate in the action. The reason for the improvement of the output performance is only electrostatic force. Under low load conditions, the load and electrostatic forces work together to significantly increase the output voltage. However, as the load force increases, the adhesion between the electrode and the polymer film becomes closer, and the role of electrostatic force in it is gradually reduced.

The next one is that the load changes cause the time nodes of each stage to change. The influence of load on the time node can be observed by comparing the output curve and topography under the same test condition of 60 r/min: first, the running-in stage time reduction. The reason is that the performance improvement of the running-in stage is due to the coupling effect of the electrostatic and load forces, and the effect of electrostatic force is weakened with the load increase. Accordingly, the running-in stage time reduction.

Second, the initial wear stage time increased from 10 min at 0 mN to 20 min at 20 mN. The reason is that the increase in output voltage at the initial stage of wear is mainly due to the increase in the actual contact area caused by wear. During the test, the film is deformed under the action of load so that it more closely bonded to the electrode contact area is increased. The bonding point of the bonding surface also increases with the increase in load. The bonding point damage under the action of abrasion is also more obvious, as shown by comparing Figures 6(b) and 6(f). Furthermore, the wound surface formed by the destruction of the bonding point increases the actual contact area and causes the output voltage to increase. The output increase time is also increased from 10 min to 20 min under the combined action of the load force and the elastic deformation of the film.

Finally, the appearance time of the severe wear stage was advanced from 80 min at 0 mN to 45 min at 20 mN. The reason is that the main wear types in the whole friction process are adhesive wear and fatigue wear. The two types of wear are more severe with the increase in load. The comparison chart is shown in Figure 6. The wear morphology map at the same time node can also confirm this view. The pitting corrosion and spalling caused by wear quickly reduce the contact area and cause the output voltage to rapidly drop, which is directly manifested as the early appearance of the severe wear stage.

3.4 Influence of Speed on the Output Voltage, Accumulated Wear Amount, Wear Morphology, and Phase Change Trend

In the Figure 7, the short-circuit current increases with the increase of speed, the open-circuit voltage

Forest Chemicals Review
www.forestchemicalsreview.com
ISSN: 1520-0191
September-October 2022 Page No. 289-305
Article History: Received: 05 April 2022, Revised: 27 April 2022, Accepted: 03 May 2022, Publication: 14 May 2022

and the transferred charge were basically the same before the severe wear stage, and later showed different decay speeds with the change of time. The greater the rotational speed, the faster the decay of the open-circuit voltage and the transferred charge. The reason for such a change is that according to the theoretical calculation formula of the amount of transferred charge and the open-circuit voltage, the magnitude of the value has nothing to do with the speed, but is only related to the actual contact area. The wear caused by the cyclic contact leads to the change of the contact area, which is the main reason for the output attenuation in the later stage. Combined with the topography diagrams in Figure 8 (a-h), which are the topographic comparison diagrams of 60 r/min and 90 r/min tests at the same time node under the same 10 mN test condition, it can be seen that, the fatigue wear phenomenon caused by continuous stress cycle is more obvious with the increase of rotation speed. The pitting and spalling phenomena are more obvious and the quality loss is more serious under the test condition of 90 r/min at the same time node, so the output attenuation is more obvious.

According to the calculation formula of the short-circuit current, the frictional contact time becomes shorter with the increase of the rotational speed. Therefore, the short-circuit current shows the same increasing trend with the increase of the speed under the condition that the amount of transferred charge is approximately the same. With the increase of rotational speed, the accumulated wear amount also showed an increasing trend. The main reason was that the increase of rotational speed increased the number of stress cycles per unit time, and accelerated the occurrence of fatigue wear, so the wear amount also followed. At the same time, with the increase of rotational speed, the time nodes of each stage appear to advance to different degrees, and each stage of acceleration occurs with the increase of rotational speed.

From the above phenomenon, we can conclude that the rotational speed has a negative effect on other electrical output and wear except short-circuit current. Therefore, the mechanical input frequency should be minimized when designing the TENG. The effect of wear on TENG can be effectively weakened while obtaining ideal open circuit voltage and charge transfer.

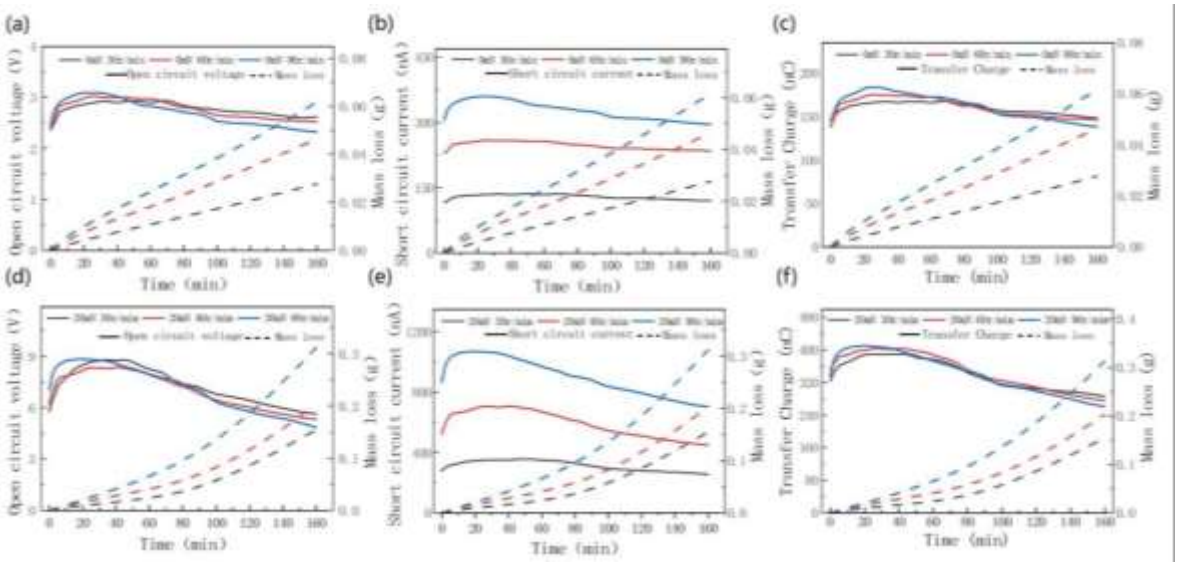

Forest Chemicals Review
www.forestchemicalsreview.com
ISSN: 1520-0191
September-October 2022 Page No. 289-305
Article History: Received: 05 April 2022, Revised: 27 April 2022, Accepted: 03 May 2022, Publication: 14 May 2022

Fig 7: The influence of different speeds on the open-circuit voltage, short-circuit current, transferred charge and mass loss under the same load. (a-c) The open-circuit voltage, short-circuit current, amount of transferred charge and accumulated wear amount vary with time at different speeds when the load is the same as 0 mN; (a-c) The open-circuit voltage, short-circuit current, amount of transferred charge and accumulated wear amount vary with time at different speeds when the load is the same as 20 mN;

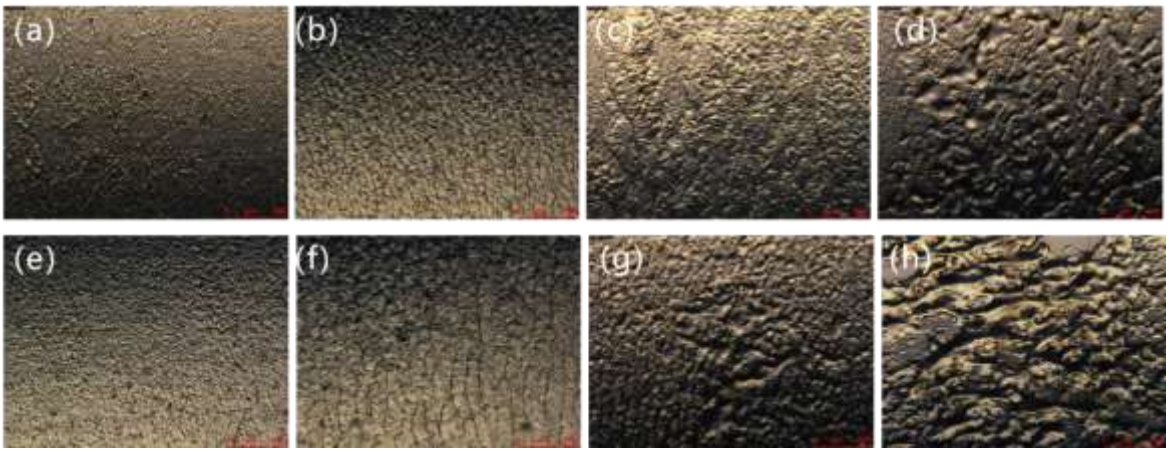

Fig 8: Comparison of surface morphologies of polymer films under the same loading conditions and different rotational speed. (a-d) Fluorescence microscope images of the surface topography of the tested 10 min, tested 70 min,tested 130 min and tested 160 min under the condition of rotating speed 60 r/min and loading 10 mN; (e-h) Fluorescence microscope images of the surface topography of the tested 10 min, tested 70 min,tested 130 min and tested 160 min under the condition of rotating speed 90 r/min and loading 10 mN

3.5 Extended Verification and Discussion

In order to verify the general applicability of the test model and conclusions, an extended test was carried out. Different dielectric layer materials and electrode materials were selected for combined testing under the same load force N=10 mN, rotational speed V=60 r/min, and film thickness d=500 μm. Six horizontal control groups are set up, and the experimental results are shown in Figure 9. In order to verify the general applicability of the test model and conclusions, an extended test was carried out. Different dielectric layer materials and electrode materials were selected for combined testing under the same load force N=10 mN, rotational speed V=60 r/min, and film thickness d=500μm. Six horizontal control groups are set up, and the experimental results are shown in Figure 9.

Forest Chemicals Review
www.forestchemicalsreview.com
ISSN: 1520-0191
September-October 2022 Page No. 289-305
Article History: Received: 05 April 2022, Revised: 27 April 2022, Accepted: 03 May 2022, Publication: 14 May 2022

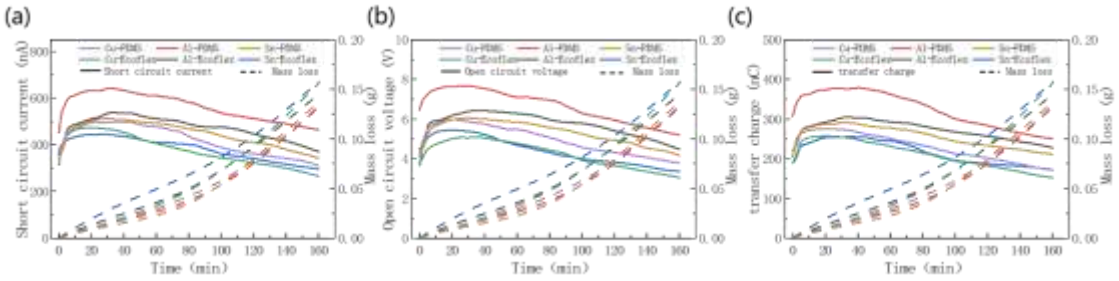

Fig 9: Curves of electrical output and cumulative wear of TENG with different combinations of electrodes and dielectric layers under the same test conditions. (a) Time-dependent curves of short-circuit current and mass loss:(b) Time-dependent curves of open-circuit voltage and mass loss:(c) Time-dependent curves of Transfer charge and mass loss.

It can be seen from the test results that although the values of open circuit voltage, short circuit current and transferred charge amount obtained after replacing the dielectric layer and electrode material are not the same, the law of change with time is similar. The experimental results are in agreement with the theoretical analysis, so the adaptability of the model and conclusions can be demonstrated.

III. CONCLUSION

This work aims to study the relationship between the tribological and the electrical properties of flexible polymers under the coupling effect of static force field. A Ecoflex00-30 typical polymer was selected as the test sample, and a friction test platform was built for testing. The main conclusions are as follows:

(1) Obvious stage changes can be observed in the electrical output and tribological characteristics during the working process of TENG, which can be divided into four phases: running-in, initial wear, stable wear, and severe wear phases. The electrical output of each stage shows good matching characteristics with the tribological characteristics. The electrical output showed an overall trend of first increasing, then tending to be stable and finally decreasing. The increase in electrical output corresponds to the running-in and the initial wear stage, and then the stable output stage corresponds to the stable wear stage. Finally, the output shows a significant downward trend due to continuous friction in and out of the severe wear stage.

(2) At the initial stage of the TENG, the output performance of charge accumulation, electrostatic adhesion and flexible deformation of the film is significantly improved, and the improvement ratio can reach up to 30%, but it will attenuate with the increase of load. Charge accumulation is an inevitable process of TENG, while the output boost caused by electrostatic adhesion effect and flexible dielectric film can be exploited, especially in the design process of flexible TENG. It can be considered to design higher output TENG structures by releasing the deformation caused by the load force and electrostatic adhesion effect of the dielectric film during its operation.

Forest Chemicals Review
www.forestchemicalsreview.com
ISSN: 1520-0191
September-October 2022 Page No. 289-305
Article History: Received: 05 April 2022, Revised: 27 April 2022, Accepted: 03 May 2022, Publication: 14 May 2022

(3) The main wear forms in the whole friction test process are adhesive wear and fatigue wear, and the amount of wear is affected by two factors: load and rotational speed. The greater the load, the greater the rotational speed, the more severe the wear. Experiments show that with the increase of rotational speed, the transferred charge and open circuit voltage of TENG will not increase, but the fatigue wear caused by the number of stress cycles will aggravate the performance degradation of TENG. Therefore, it should be biased towards low-frequency working conditions in the design of TENG, with ideal output and stronger durability.

ACKNOWLEDGEMENTS

This work is supported by the National Natural Science Foundation of China (Grant Nos. 51675236), Jiangsu industry prospect project (SBE2021030339), Independent innovation fund of Jiangsu Agricultural Committee (CX(20)2024), Qing Lan Project of Jiangsu Province(2021).

REFERENCES

[1] Tao K, Yi H, Yang Y, Chang H, Wu J, Tang L, Yang Z, Wang N, Hu L, Fu Y (2020) Origami-inspired electret-based triboelectric generator for biomechanical and ocean wave energy harvesting. Nano Energy 67: 104197

[2] Li K, Wu Y S, Liu Q, Cheng G G, Zhang Z Q, Guo L Q, Wang Y, Ding J N (2018) Rotational Triboelectric Nanogenerator Based on a PDMS@CS Composite Material. Journal of Physical Chemistry C 122(43): 24578-24584

[3] Cao J, Gu W G, Qu Z Q, Zhong Y, Cheng G G, Zhang Z Q (2020) Design and research of non-contact triboelectric nanogenerator based on changing electrostatic field. Acta Physica Sinica 69(23): 230201

[4] Cheng G G, Zhang W, Fang J, Jiang S Y, Ding J N, Pesika N S, Zhang Z Q, Guo L Q, Wang Y (2016) Fabrication of triboelectric nanogenerator with textured surface and its electric output performance. Acta Physica Sinica 65(6): 060201

[5] Cheng G G, Jiang S Y, Li K, Zhang Z Q, Wang Y, Yuan N Y, Ding J N, Zhang W (2017) Effect of argon plasma treatment on the output performance of triboelectric nanogenerator. Applied Surface Science 412: 350-356

[6] Wang J, Wu C S, Dai Y J, Zhao Z H, Wang A, Zhang T J, Wang Z L (2017) Achieving ultrahigh triboelectric charge density for efficient energy harvesting. Nature Communications 8: 88

[7] Wang Y, Wu Y, Liu Q, Wang X, Cao J, Cheng G, Zhang Z, Ding J, Li K (2020) Origami triboelectric nanogenerator with double-helical structure for environmental energy harvesting. Energy 212: 118462

[8] Zhao Z, Pu X, Du C, Li L, Jiang C, Hu W, Wang Z L (2016) Freestanding Flag-Type Triboelectric Nanogenerator for Harvesting High-Altitude Wind Energy from Arbitrary Directions. Acs Nano 10(2): 1780-1787

[9] Wu Y S, Liu Q, Cao J, Li K, Cheng G G, Zhang Z Q, Ding J N, Jiang S Y (2019) Design and output performance of vibration energy harvesting triboelectric nanogenerator. Acta Physica Sinica 68(19): 190201

[10] Wang X, Niu S, Yi F, Yin Y, Hao C, Dai K, Zhang Y, You Z, Wang Z L (2017) Harvesting Ambient Vibration Energy over a Wide Frequency Range for Self-Powered Electronics. Acs Nano 11(2): 1728-1735

[11] Wang X F, Niu S M, Yi F, Yin Y J, Hao C L, Dai K, Zhang Y, You Z, Wang Z L (2017) Harvesting Ambient Vibration Energy over a Wide Frequency Range for Self-Powered Electronics. Acs Nano 11(2): 1728-1735

Forest Chemicals Review
www.forestchemicalsreview.com
ISSN: 1520-0191
September-October 2022 Page No. 289-305
Article History: Received: 05 April 2022, Revised: 27 April 2022, Accepted: 03 May 2022, Publication: 14 May 2022

[12] Dong K, Wu Z, Deng J, Wang A C, Zou H, Chen C, Hu D, Gu B, Sun B, Wang Z L (2018) A Stretchable Yarn Embedded Triboelectric Nanogenerator as Electronic Skin for Biomechanical Energy Harvesting and Multifunctional Pressure Sensing. Advanced Materials 30(43): 1804944
[13] Lin Z, Chen J, Li X, Zhou Z, Meng K, Wei W, Yang J, Wang Z L (2017) Triboelectric Nanogenerator Enabled Body Sensor Network for Self-Powered Human Heart-Rate Monitoring. Acs Nano 11(9): 8830-8837
[14] Xue H, Yang Q, Wang D Y, Luo W J, Wang W Q, Lin M S, Liang D L, Luo Q M (2017) A wearable pyroelectric nanogenerator and self-powered breathing sensor. Nano Energy 38: 147-154
[15] Shi Q F, He T Y Y, Lee C (2019) More than energy harvesting - Combining triboelectric nanogenerator and flexible electronics technology for enabling novel micro-/nano-systems. Nano Energy 57: 851-871
[16] Zhou L L, Liu D, Wang J, Wang Z L (2020) Triboelectric nanogenerators: Fundamental physics and potential applications. Friction 8(3): 481-506
[17] Li S, Nie J, Shi Y, Tao X, Wang F, Tian J, Lin S, Chen X, Wang Zhong L (2020) Contributions of Different Functional Groups to Contact Electrification of Polymers. Advanced Materials 32(25): 2001307
[18] Yang J, Yang F, Zhao L, Shang W, Qin H, Wang S, Jiang X, Cheng G, Du Z (2018) Managing and optimizing the output performances of a triboelectric nanogenerator by a self-powered electrostatic vibrator switch. Nano Energy 46: 220-228
[19] Du J, Duan J, Yang X, Wang Y, Duan Y, Tang Q (2020) Charge boosting and storage by tailoring rhombus all-inorganic perovskite nanoarrays for robust triboelectric nanogenerators. Nano Energy 74: 104845
[20] Liu Y, Mo J, Fu Q, Lu Y, Zhang N, Wang S, Nie S (2020) Enhancement of Triboelectric Charge Density by Chemical Functionalization. Advanced Functional Materials 30(50): 2004714
[21] Shang W Y, Gu G Q, Yang F, Zhao L, Cheng G, Du Z L, Wang Z L (2017) A Sliding-Mode Triboelectric Nanogenerator with Chemical Group Grated Structure by Shadow Mask Reactive Ion Etching. Acs Nano 11(9): 8796-8803
[22] Wang P, Pan L, Wang J, Xu M, Dai G, Zou H, Dong K, Wang Z L (2018) An Ultra-Low-Friction Triboelectric-Electromagnetic Hybrid Nanogenerator for Rotation Energy Harvesting and Self-Powered Wind Speed Sensor. Acs Nano 12(9): 9433-9440
[23] Lin Z M, Zhang B B, Zou H Y, Wu Z Y, Guo H Y, Zhang Y, Yang J, Wang Z L (2020) Rationally designed rotation triboelectric nanogenerators with much extended lifetime and durability. Nano Energy 68: 104378
[24] Xu L, Bu T Z, Yang X D, Zhang C, Wang Z L (2018) Ultrahigh charge density realized by charge pumping at ambient conditions for triboelectric nanogenerators. Nano Energy 49: 625-633
[25] Li X, Yin X, Zhao Z, Zhou L, Liu D, Zhang C, Zhang C, Zhang W, Li S, Wang J (2020) Long-Lifetime Triboelectric Nanogenerator Operated in Conjunction Modes and Low Crest Factor. Advanced Energy Materials 10(7): 1903024
[26] Zhang J, Zheng Y, Xu L, Wang D (2020) Oleic-acid enhanced triboelectric nanogenerator with high output performance and wear resistance. Nano Energy 69: 104435
[27] Wu J, Xi Y, Shi Y (2020) Toward wear-resistive, highly durable and high performance triboelectric nanogenerator through interface liquid lubrication. Nano Energy 72: 104659
[28] Jin C R, Kia D S, Jones M, Towfighian S (2016) On the contact behavior of micro-/nano-structured interface used in vertical-contact-mode triboelectric nanogenerators. Nano Energy 27: 68-77
[29] Harris K L, Pitenis A A, Sawyer W G, Krick B A, Blackman G S, Kasprzak D J, Junk C P (2015) PTFE Tribology and the Role of Mechanochemistry in the Development of Protective Surface Films. Macromolecules 48(11): 3739-3745
[30] Niu S, Liu Y, Chen X, Wang S, Zhou Y S, Lin L, Xie Y, Wang Z L (2015) Theory of freestanding triboelectric-layer-based nanogenerators. Nano Energy 12: 760-774

Forest Chemicals Review
www.forestchemicalsreview.com
ISSN: 1520-0191
September-October 2022 Page No. 289-305
Article History: Received: 05 April 2022, Revised: 27 April 2022, Accepted: 03 May 2022, Publication: 14 May 2022

[31] Shao J, Jiang T, Tang W, Xu L, Kim T W, Wu C, Chen X, Chen B, Xiao T, Bai Y (2018) Studying about applied force and the output performance of sliding-mode triboelectric nanogenerators. Nano Energy 48: 292-300
[32] Archard J F (1953) Contact and Rubbing of Flat Surfaces. Journal of Applied Physics 24(8): 981-988.